ISSN 1063-7761, Journal of Experimental and Theoretical Physics, 2016, Vol. 122, No. 2, pp. 298–309. © Pleiades Publishing, Inc., 2016.
Original Russian Text © V.E. Ankudinov, P.K. Galenko, N.V. Kropotin, M.D. Krivilyov, 2016, published in Zhurnal Eksperimental'noi i Teoreticheskoi Fiziki, 2016, Vol. 149, No. 2, pp. 343–356.

SOLIDS AND LIQUIDS

Atomic Density Functional and Diagram of Structures in the Phase Field Crystal Model

V. E. Ankudinov[a], P. K. Galenko[b,c], N. V. Kropotin[a], and M. D. Krivilyov[a]

[a] *Udmurt State University, Izhevsk, 426034 Russia*
[b] *Ural Federal University, Yekaterinburg, 620002 Russia*
[c] *Friedrich-Schiller-Universität Jena, Physikalisch-Astronomische Fakultät, Jena, D-07743 Germany*
e-mail: vladimir@ankudinov.org

Received August 12, 2015

Abstract—The phase field crystal model provides a continual description of the atomic density over the diffusion time of reactions. We consider a homogeneous structure (liquid) and a perfect periodic crystal, which are constructed from the one-mode approximation of the phase field crystal model. A diagram of 2D structures is constructed from the analytic solutions of the model using atomic density functionals. The diagram predicts equilibrium atomic configurations for transitions from the metastable state and includes the domains of existence of homogeneous, triangular, and striped structures corresponding to a liquid, a body-centered cubic crystal, and a longitudinal cross section of cylindrical tubes. The method developed here is employed for constructing the diagram for the homogeneous liquid phase and the body-centered iron lattice. The expression for the free energy is derived analytically from density functional theory. The specific features of approximating the phase field crystal model are compared with the approximations and conclusions of the weak crystallization and 2D melting theories.

DOI: 10.1134/S1063776116020011

1. INTRODUCTION

The phase field crystal model [1–3] was formulated to describe continual transitions from the homogeneous to the periodic state (similar to the Landau–Brazovskii transition [4–7]) and between different periodic states over diffusion times [8]. The model is based on the description of the free energy, which is a functional of the atomic density field n-periodic in the solid phase and homogeneous in the liquid state.

Periodicity n of the field takes into account the elastic properties and multiplicity of crystallographic orientations of the atomic continuum, which is described by the equation of motion for the average value of conservative order parameter n_0. This makes it possible to simulate a wide class of phenomena including, e.g., epitaxial growth and ordering of nanostructures on micrometer scales [8], crystallization and high-speed regimes of front propagation [9, 10], the motion of dislocations and plastic flow, the formation of a disordered amorphous state, premelting of grain boundaries, crack spreading, rearrangement of microscopic structure of interfaces, and the dynamics of colloidal systems and polymers (see [11]).

The determination of equilibrium structures and their coexistence in "average atomic density–temperature" and "average atomic density–transition driving force" diagrams occupies a special place in the phase field model. Such diagrams are required for determining the structures to which unstable or metastable states must evolve. Diagrams of 2D structures for transitions from an unstable state were constructed in detail using the atomic density functional and the Maxwell equal-area rule [2, 12]. The structural diagram for transitions from the metastable state was also constructed earlier, but in a narrower range of the control parameter [13]. The dynamics of systems with the formation of periodic crystalline structures is studied in a wide range of control parameters [14]. Therefore, determination of the domains of existence of stable structures in equilibrium in a wide range of parameters is a topical problem in phase field theory [13].

In this study, we formulate a method for constructing the diagram of 2D structures for transitions from a metastable state to a periodic phase for arbitrary values of the driving force and atomic density. This method makes it possible to determine the parameter range for the existence of 3D structures. This is demonstrated using the phase diagram of a body-centered cubic (bcc) iron lattice and a homogeneous liquid phase.

2. FREE ENERGY

As the driving force, we choose control parameter $\Delta B_0 = B_0^\ell - B_0^x$, which determines the difference

between compressibility B_0^ℓ of the liquid and elastic modulus B_0^x (in dimensionless units, see [8, 14]). Transition from the metastable state is possible if compressibility B_0^ℓ exceeds elastic modulus B_0^x so that $\Delta B_0 = B_0^\ell - B_0^x > 0$. If, however, compressibility B_0^ℓ becomes smaller than elastic modulus B_0^x (i.e., $\Delta B_0 = B_0^\ell - B_0^x < 0$), a transition from an unstable state is possible. For definiteness, we consider only transitions from the metastable to the stable phase (i.e., for $\Delta B_0 > 0$). Finally, for dimensionless atomic density, we choose parameter $n \equiv (\rho - \overline{\rho})/\overline{\rho}$, where $\overline{\rho}$ is the local atomic density and $\overline{\rho}$ is the constant atomic density of the liquid chosen as the reference density. Atomic density n in the model described below is a conservative (conserved) order parameter.

For an isothermal one-component system, we choose the free energy in the form of the functional [13]

$$F(n,T) = \int_V dV \left(\Delta B_0 \frac{n^2}{2} + B_0^x \frac{n}{2} \mathfrak{D}_i n - 2a \frac{n^3}{3} + 15v \frac{n^4}{4} \right), \quad (1)$$

where operator $\mathfrak{D}_i$ for $i = 1$ and $i = 2$ describes the one-mode approximation

$$\mathfrak{D}_i \equiv \mathfrak{D}_1 = (1 + R_1^2 \nabla^2)^2 \quad (2)$$

or the two-mode approximation

$$\mathfrak{D}_i \equiv \mathfrak{D}_2 = [R_2 + (Q_2 + R_1^2 \nabla^2)^2](1 + R_1^2 \nabla^2)^2. \quad (3)$$

Free energy (1) is a specific (per unit volume) functional normalized to $k_B T \overline{\rho}$, where k_B is the Boltzmann constant, T is the temperature, $\overline{\rho}$ is (as defined above) the reference density chosen as the constant atomic density of the liquid, ΔB_0 and B_0^x are coefficients, and a and v are phenomenological parameters that can be selected for certain properties of the material [15–17]. The values of R_1, R_2, and Q_2 in operators (2) and (3) are calculated in terms of the coefficients of the atomic density correlation function for the unit cell with lattice vector $\mathbf{q}_1$ in the case of the one-mode approximation or using a second-order cell with lattice vector $\mathbf{q}_2$ in the case of the two-mode approximation [18, 19]. With allowance for only one parameter $\mathbf{q}_1$ determined in the first approximation by the two-point correlation function of atoms [18], one-mode approximation (2) describes, e.g., a simple cubic or bcc lattice [15]. When two-mode approximation (3) is used, two characteristic lattice parameters are taken into account, which is the next approximation of the atomic correlation function (or of the static structural factor). The two-mode approximation makes it possible to describe finer structures (e.g., a face-centered or hexagonal close-packed crystal lattice) [20, 21]. Thus, 3D operators (2) and (3) take into account the lowest and higher approximations, respectively, and describe different degrees of complexity of the crystal structure. As a result of these approximations, the functional makes it possible to describe systems on the scale of atomic lengths and on the scale of the diffusion times of atoms (i.e., it obviously cannot be used in analyzing atomic systems on the atomic vibration scale) [13]. For this reason, the periodic states and the dynamics of transitions between them can be predicted with this functional on scales occupying positions between the scales of standard phenomenological phase-field models and discrete atomistic models (such as the molecular dynamics model or density functional theory) [3].

Functional (1) has the form which was used in the formulation and development of the "weak" crystallization theory [6] for describing a system with the conserved order parameter, as well as for convective instability according to the Swift–Hohenberg theory [9, 13] in analysis of the evolution of nonpersistent order parameters. In the general case, free energy (1) provides a description of a stable or metastable system that can experience a first-order phase transition precisely due to the presence of the cubic term in its integrand [4, 22, 23]. A second-order phase transition can also be described in the phase field crystal model, but for $a = 0$ (i.e., without the cubic term in free energy (1)). E.g., analysis of marginal instability and the selection of the structural parameter of lamellas in diblock copolymers [10] are associated with precisely a second-order phase transition with $a = 0$ in the free energy. Let us now demonstrate analytically the difference in the description of the second- and first-order phase transitions in the phase field model.

Considering the integrand in functional (1), we can write free energy density $f(n, T)$ in the form

$$f(n,T) = f_0(T) + B_0^x \frac{n}{2} \mathfrak{D}_i n + \Delta B_0 \frac{n^2}{2} - 2a \frac{n^3}{3} + 15v \frac{n^4}{4}, \quad (4)$$

where $f_0(T)$ is the Helmholtz free energy density for the high-temperature phase ($n = 0$, $\rho = \overline{\rho}$). Free energy density (4) for the homogeneous high-temperature phase in which $\mathfrak{D}_i n = 0$ determines the equation of state from the condition $\partial f/\partial n = 0$ in the form

$$\Delta B_{0m} n - 2an^2 + 15vn^2 = 0. \quad (5)$$

Provided that $\Delta B_{0m} = B_{0m}^\ell - B_0^x$ is the difference between the critical value of compressibility B_{0m}^ℓ and elastic modulus B_0^x required for the formation of a metastable liquid, the roots of Eq. (5) are given by

$$n_1 = 0, \quad n_{2,3} = \frac{a \pm \sqrt{a^2 - 15v\Delta B_{0m}}}{15v}. \quad (6)$$

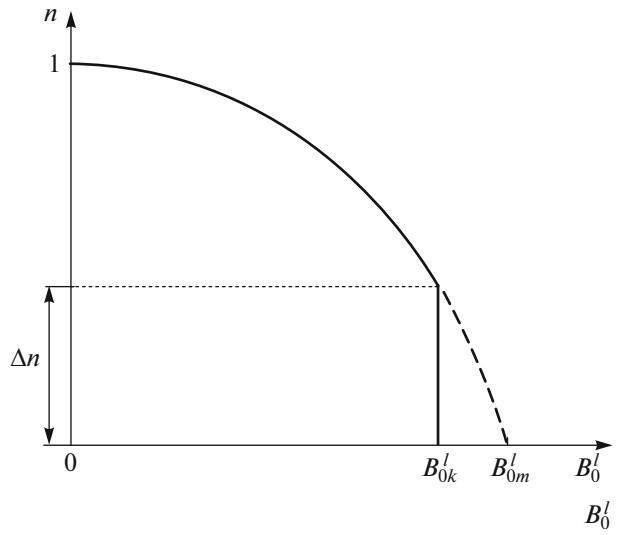

Fig. 1. Variation in the conservative order parameter (atomic density n) in the phase field crystal model. Continuous variation in n in the second-order transition (dashed curve beginning from B_{0m}^ℓ and transformed into the solid curve) is demonstrated; discontinuous (jumpwise) variation in n in the first-order transition (solid line beginning from B_{0k}^ℓ). Density jump Δn is determined by expression (11) for $a \neq 0$, and continuous variation in n is also determined by Eq. (11), but for $a = 0$ and for $B_{0k}^\ell = B_{0m}^\ell$.

The real-valued solution from the set of densities (6) can be determined from the physically admissible condition $n_2 = n_3$, i.e., for

$$\Delta B_{0m} = \frac{a^2}{15v}, \quad B_{0m}^\ell = B_0^x + \frac{a^2}{15v}. \tag{7}$$

If $B_0^\ell > B_{0m}^\ell$, only one homogeneous state is stable for $n = 0$. For $B_0^\ell < B_{0m}^\ell$, a metastable minimum appears for $n \neq 0$.

The phase transition point is determined by the condition of equality of energies $f(n, T) = f_0(T)$. Then expression (4) gives the equation

$$\frac{\Delta B_{0k}}{2} n^2 - \frac{2a}{3} n^3 + \frac{15v}{4} n^4 = 0, \tag{8}$$

with the roots

$$n_1 = 0,$$
$$n_{2,3} = \frac{2}{15v}\left(\frac{2a}{3} \pm \sqrt{\frac{4a^2}{9} - \frac{15v\Delta B_{0k}}{2}}\right), \tag{9}$$

where $\Delta B_{0k} = B_{0k}^\ell - B_0^x$ is the difference between the critical value of compressibility B_{0k}^ℓ and elastic modulus B_0^x. The real values of density (9) are observed for $n_2 = n_3$, which leads to the conditions

$$\Delta B_{0k} = \frac{8a^2}{135v}, \quad B_{0k}^\ell = B_0^x + \frac{8a^2}{135v}. \tag{10}$$

Here, B_{0k}^ℓ is the critical compressibility value required for crystallization of the metastable liquid phase.

Expressions (7) and (10) show that to initiate crystallization, the compressibility of the liquid phase must be lower than the compressibility required for the occurrence of metastability (i.e., $B_{0k}^\ell < B_{0m}^\ell$). This means that upon cooling of the high-temperature phase, a metastable liquid appears first, and only then the phase transition point is attained at which, under condition (10), we obtain the equality $B_0^\ell = B_{0k}^\ell$ and two stable states for density: $n = n_0$ and $n \neq 0$.

The condition $B_{0k}^\ell < B_{0m}^\ell$ leads to a discontinuous (jumpwise) variation in density at the phase transition point. Indeed, using expressions (6), (9), and (10), we obtain

$$\Delta n\,|_{B_0^\ell = B_{0t}^\ell} = n(B_{0k}^\ell) - n(B_{0m}^\ell) = n(B_{0k}^\ell) - 0$$
$$= \frac{2}{15v}\left(\frac{2a}{3} \pm \sqrt{\frac{4a^2}{9} - \frac{15v\Delta B_{0k}}{2}}\right) = \frac{4a}{45v}. \tag{11}$$

Figure 1 shows density jump (11) at the phase transition point. The jumpwise variation in density is one of the basic characteristics of a first-order transition [4, 22, 23], which is due to the presence of the cubic term in free energy density (4). For $a = 0$, the contribution of the cubic term in free energy density (4) vanishes, and we then obtain $B_{0k}^\ell = B_{0m}^\ell$ (see expressions (7) and (10)). In this case, the density at the transition point varies continuously (without a jump): $n(B_{0k}^\ell) = n(B_{0m}^\ell)$ (see expression (11) for $a = 0$). Such a continuous variation in density is one of the basic characteristics of a second-order transition [4, 22, 23], which is due to the cubic term in energy (4). The continuous variation in density (11) for $a = 0$ is also shown in Fig. 1.

For specific crystalline structures and liquids, physical parameters B_0^ℓ, B_0^x, a, and v in functional (1) can be determined, e.g., from the atomic distribution functions and atomic density distribution functions obtained using the molecular dynamics method [18]. In this study, we use molecular dynamics simulation data to determine the physical parameters of the free energy and construct the structural diagram of iron (see Section 5).

3. STRUCTURAL STATES

Analogously to the results obtained in [12], we assume that using free energy (1) to determine stable structural states in the 2D space, we can find the allowed domains of existence of the states of a

(i) homogeneous structure (liquid);

(ii) triangular structure;

(iii) striped structure;

as well as the domains of existence of

(iv) a homogeneous–triangular structure;

(v) triangular–striped structure.

We construct the structural diagram in an arbitrary range of control parameters $0 \leqslant \Delta B_0 \leqslant 0.9$ according to the calculations performed below. It should be noted for comparison that the structural diagram for first-order transitions is constructed in the limited range $0 \leqslant \Delta B_0 \leqslant 0.12$ (see Figs. 8.12 and 8.13 in [13]).

In static equilibrium, the solutions to the equation

$$\nabla^2(\Delta B_0 n + B_0^x \mathfrak{D}_i n - 2an^2 + 15vn^3) = 0 \qquad (12)$$

ensure the minimization of free energy (1). The general solution to Eq. (12) for atomic density n can be written in the form

$$n = n_0 + \sum_{klm} \eta_{klm} \exp(i\mathbf{G}_{klm} \cdot \mathbf{r}) + \sum_{klm} \eta^*_{klm} \exp(-i\mathbf{G}_{klm} \cdot \mathbf{r}) \equiv n_0 + \sum_{klm} [\eta_{klm} \exp(i\mathbf{G}_{klm} \cdot \mathbf{r}) + \text{c.c.}], \qquad (13)$$

where the 3D crystalline structure is characterized by the vector

$$\mathbf{G}_{klm} = k\mathbf{q}_1 + l\mathbf{q}_2 + m\mathbf{q}_3, \qquad (14)$$

required to reproduce low-order wavevectors for the given symmetry. Vectors $\mathbf{q}_1$, $\mathbf{q}_2$, and $\mathbf{q}_3$ are the reciprocal lattice vectors; k, l, and m are the Miller indices; η_{klm} is the complex amplitude; η^*_{klm} is a function complex-conjugate to η_{klm}; n_0 is the average atomic density; and "c.c." is the contribution from complex-conjugate functions. Although the densities of the crystal and the liquid are different, we assume for simplicity that n_0 is a constant. Indeed, to determine the exact compliance with the solutions in equilibrium, we must use all integer values of k, l, and m; however, in the vicinity of the liquid–crystal transition temperature, disregard of the difference in densities of the phases is an admissible approximation for the model in which only low-order contributions are taken into account. The specific representation of each phase in accordance with expression (13) and its substitution into the general expression (1) for the free energy make it possible to determine the specific form of the functional by minimization in the amplitude and the reciprocal crystal lattice parameter. Then the diagram of the regions of coexistence of the structures can be constructed from the condition of the equality of the chemical potentials in thermodynamic equilibrium using the Maxwell equal-area rule [2, 12]. In our calculations of free energy (1) for a specific atomic structure, only the one-mode approximation $\mathfrak{D}_i = \mathfrak{D}_1$ in accordance with expression (2) is used.

3.1. Homogeneous Structure

Liquid as a homogeneous structure is a system without a long-range order of interaction, in which the structural disorder is defined by zero reciprocal lattice vectors:

$$\mathbf{q}_1 = 0, \quad \mathbf{q}_2 = 0, \quad \mathbf{q}_3 = 0. \qquad (15)$$

The solution to Eq. (12) in the form of the amplitude representation (13) and (14) in the entire domain of existence of the liquid degenerates to the average atomic density n_0; i.e.,

$$n = n_0. \qquad (16)$$

To determine the free energy of the liquid, we substitute this expression into free energy functional (1). The resultant expression should be integrated over the unit cell volume; however, since the unit cell for the homogeneous phase does not exist as such, its size can be defined arbitrarily. Therefore, for a characteristic scale of $a_{\text{eq}} = 2\pi/q$ with wavenumber q, we obtain the specific free energy of the liquid in the form

$$F_h(n_0, \Delta B_0) = B_0^{\ell} \frac{n_0^2}{2} - 2a\frac{n_0^3}{3} + 15v\frac{n_0^4}{4}, \qquad (17)$$

where subscript "h" indicates the homogeneous structure (viz., liquid).

3.2. Triangular Structure

In the 2D case, the triangular structure is the cross section of a body-centered crystal in the {110} plane (see Fig. 2), or the cross section of triangularly packed rods (Fig. 3). Using lattice parameter a_{eq} and lattice wavenumber $q = 2\pi/a_{\text{eq}}$, we write the reciprocal lattice vectors for the triangular structure:

$$\mathbf{q}_1 = -q\left(\frac{\sqrt{3}}{2}\mathbf{i}_1 + \frac{1}{2}\mathbf{i}_2\right), \quad \mathbf{q}_2 = q\mathbf{i}_2, \quad \mathbf{q}_3 = 0, \qquad (18)$$

where $\mathbf{i}_1$ and $\mathbf{i}_2$ are unit vectors. Vector $\mathbf{G}_{klm}$ defined by expression (14) for the 2D space has the form $m\mathbf{q}_3 = 0$ for the lowest order of the coefficients of the reciprocal lattice vectors:

$$(k,l) = (1,0); \quad (0,1); \quad (-1,-1). \qquad (19)$$

Assuming for convenience of calculations that amplitudes $\eta_{klm} = 4\eta$, we can reduce general wave solution (13) and (14) for the triangular structure to the form

$$n = n_0 + 4\eta\left[\frac{1}{2}\cos(qy) - \cos\left(\frac{\sqrt{3}}{2}qx\right)\cos\left(\frac{q}{2}y\right)\right]. \qquad (20)$$

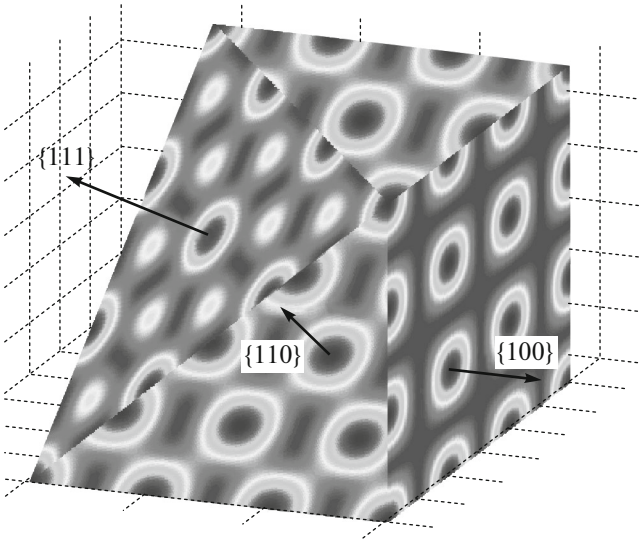

Fig. 2. Distribution of the atomic density of the body-centered crystal lattice and its sections in the {111}, {110}, and {100} planes. Calculations were performed with Eq. (13) with coefficients (45) corresponding to the vectors of the body-centered lattice. In the section by the {110} plane, the triangular structure described by Eqs. (25) for the regions of triangles in Fig. 4 can clearly be seen.

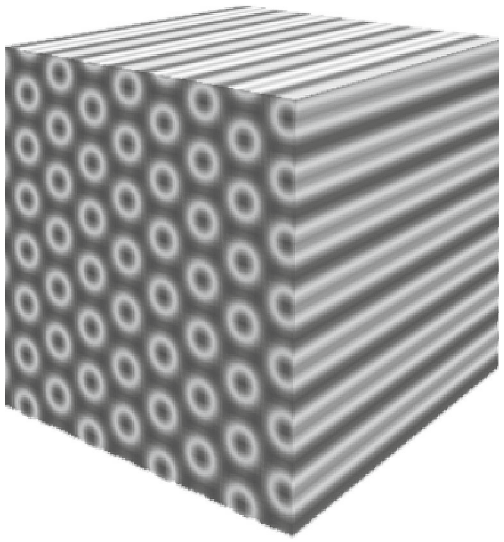

Fig. 3. Atomic density distribution in the form of the rod structure. Calculations were performed with Eq. (13) with coefficients (25) corresponding to the reciprocal lattice vectors of the rod structure. The faces of the cube show the cross sections with the 2D hexagonal and striped structures. The striped structure corresponds to the stripe region in Fig. 4.

Comparing this expression with the analogous form of the amplitude representation of the triangular structure (expression (40) from [12]),

$$n_t = A_t \cos(q_t x)\cos\left(\frac{q_t y}{\sqrt{3}}\right) - \frac{A_t}{2}\cos\left(\frac{2q_t y}{\sqrt{3}}\right) + n_0,$$

we see that these expressions are identical if the following substitution is used: $q = 2q_t/\sqrt{3}$ and $A_t = 4\eta$.

Taking into account the amplitude representation (20) of the triangular structure, we can write free energy (1) for the spatial region corresponding to the unit cell volume in the triangular structure:

$$F(n,T) = \int_0^{2\pi/\sqrt{3}q} \frac{\sqrt{3}q}{2\pi}dx \int_0^{2\pi/q} \frac{q}{2\pi}dy \int_0^{2\pi/q} \frac{q}{2\pi}dz \times\left(B_0^{\ell}\frac{n^2}{2} + B_0^{x}\frac{n}{2}(2\nabla^2 + \nabla^4)n - 2a\frac{n^3}{3} + 15v\frac{n^4}{4}\right). \quad (21)$$

The choice of integration limits in this expression is determined by the sizes of the unit cell of the periodic structure. It should also be noted that operator ∇ has already been scaled to coefficient R_1.

Minimizing now free energy (21) in wavenumber q, we obtain its equilibrium values $q_{eq} = 0, 1, -1$. Since only the wavenumber $q = q_{eq} = 1$ has physical meaning, we substitute it into expression (21) for the free energy. As a result, the free energy of the triangular structure assumes the form

$$F_{tr}(n_0,\eta) = \eta^2(3\Delta B_0 - 12an_0 + 135vn_0^2) + \eta^3(-8a + 180vn_0) + \eta^4\frac{675}{2}v + B_0^{\ell}\frac{n_0^2}{2} - 2a\frac{n_0^3}{3} + 15v\frac{n_0^4}{4}, \quad (22)$$

where subscript "tr" indicates the triangular structure. Minimizing further expression (22) in amplitude η, we obtain

$$\frac{\partial F_{tr}(n_0,\eta)}{\partial\eta} = \eta(-24an_0 + 270n_0^2 + 6\Delta B_0) + \eta^2(-24a + 540vn_0) + \eta^3 180vn_0 = 0. \quad (23)$$

This equation has the following roots:

$$\eta = 0;\quad \frac{2a - 45vn_0}{225v} \pm \frac{(4a^2 + 720avn_0 - 8100v^2n_0^2 - 225v\Delta B_0)^{1/2}}{225v}. \quad (24)$$

From this set of values, we choose only the positive root (as having physical meaning) and substitute it into Eq. (22). This gives the final form of free energy functional $F_{tr}(n_0, \Delta B_0)$ of the triangular structure.

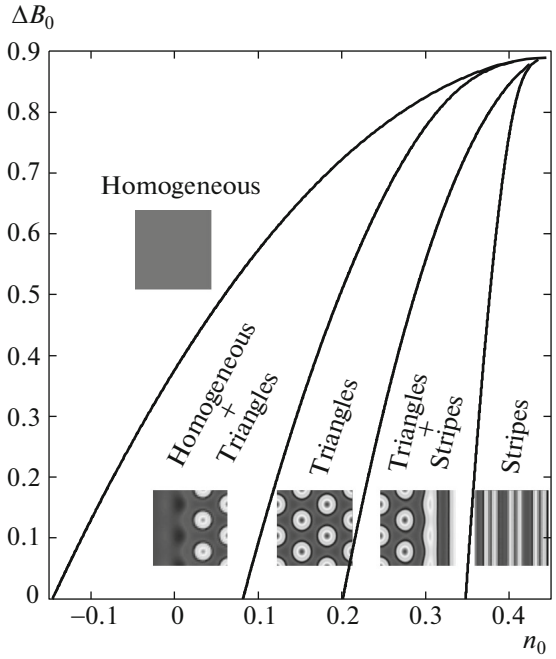

Fig. 4. Diagram of coexistence of homogeneous, triangular, and striped structures in a wide range of control parameter ΔB_0. Parameters $a = 1$, $v = 0.1$, and $B_0^\ell = 1$ for solving system (30) were borrowed from [14].

3.3. Striped Structure

The striped structure is a 2D projection of the layered 3D periodic structure (see Fig. 3). The reciprocal lattice vectors for the striped structure have the form

$$\mathbf{q}_1 = q\mathbf{i}_1, \quad \mathbf{q}_2 = 0, \quad \mathbf{q}_3 = 0. \tag{25}$$

Using the general wave solutions (13) and (14), we can write the partial amplitude representation for the striped structure in the form

$$n = n_0 + 4\eta\cos(qx). \tag{26}$$

To determine the free energy of the striped structure, we write the integration limits and substitute amplitude representation (26) into functional (1):

$$F(n,T) = \int_0^{2\pi/q}\frac{q}{2\pi}dx\int_0^{2\pi/q}\frac{q}{2\pi}dy\int_0^{2\pi/q}\frac{q}{2\pi}dz \times\left(B_0^\ell\frac{n^2}{2} + B_0^x\frac{n}{2}(2\nabla^2+\nabla^4)n - 2a\frac{n^3}{3} + 15v\frac{n^4}{4}\right). \tag{27}$$

It should also be noted here that operator ∇ has already been scaled to coefficient R_1. Further, we minimize free energy (27) in q and find $q_{eq} = 0, 1, -1$. Hence, it follows that for $q_{eq} = 1$, free energy (27) assumes the form

$$F_{str}(n_0,\eta) = \eta^2(4\Delta B_0 - 16an_0 + 180vn_0^2) + \eta^4 360v + B_0^\ell\frac{n_0^2}{2} - 2a\frac{n_0^3}{3} + 15v\frac{n_0^4}{4}, \tag{28}$$

where subscript "str" denotes the striped structure. Minimizing now expression (28) in η, we obtain the roots

$$\eta = 0; \quad \pm\frac{\sqrt{5}\sqrt{v(4an_0 - 45v^2n_0^2 - \Delta B_0)}}{30v}. \tag{29}$$

Choosing the positive root and substituting it into free energy (28), we obtain the final form of free energy $F_{str}(n_0, \Delta B_0)$ for the striped structure.

4. DIAGRAM OF 2D STRUCTURES

Having determined the structural states (see Section 3), we construct the diagram of the coexistence of 2D structures in terms of the expressions for the free energies derived above for each phase, viz., $F_h(n_0, \Delta B_0)$, $F_{tr}(n_0, \Delta B_0)$, and $F_{str}(n_0, \Delta B_0)$. For this, we write the Maxwell area rule [2, 12] and solve the equations for the entire range of control parameter values $0 \leqslant \Delta B_0 \leqslant 0.9$:

$$\begin{aligned}\mu_{tr}(n_{0tr},\Delta B_0) &= \mu_h(n_{0h},\Delta B_0),\\ F_{tr} - F_h &= \mu_h(n_{0h},\Delta B_0)(n_{0tr} - n_{0h}),\\ \mu_{tr}(n_{0tr},\Delta B_0) &= \mu_{str}(n_{0str},\Delta B_0),\\ F_{tr} - F_{str} &= \mu_{str}(n_{0str},\Delta B_0)(n_{0tr} - n_{0h}).\end{aligned} \tag{30}$$

In this set of equations, the chemical potential of the given structure is defined as $\mu \equiv \partial F/\partial n|_{n=n_0}$.

The visualization of the solutions to system of equations (30) is shown in Fig. 4. The figure depicts the diagram of equilibrium structures to which the metastable states should evolve for the given values of control parameter ΔB_0 and average atomic density n_0. It can be seen from Fig. 4 that for each chosen interval of values of parameters $(\Delta B_0, n_0)$, only a certain structure can exist or two structures can coexist. Indeed, for a certain fixed value of ΔB_0, a gradual increase in average density n_0 leads to a structure with increasing density in equilibrium: liquid $\rightarrow$ triangular structure $\rightarrow$ striped structure. If we fix density n_0 and increase parameter ΔB_0, we obtain a transition to a homogeneous state (i.e., liquid). Since parameter ΔB_0 characterizes extension in the system (as the difference between the compressibility and the elastic modulus), the energetically most advantageous structure for the highest values of parameter ΔB_0 is the structure with the largest distance between atoms (i.e., the liquid is ultimately formed). It should also be noted that the choice of values of coefficients a and v in the free energy considerably affects the admissible values of parameters $(\Delta B_0, n_0)$. Therefore, to describe crystals of

different systems, the determination of these coefficients is of primary importance [18].

5. DIAGRAM OF 3D STRUCTURES

Using the method for constructing the diagram of 2D structures (see Section 4), we can demonstrate its applicability for the 3D case of coexistence of a homogeneous liquid and a bcc lattice using iron melt and crystal as an example. It should be noted, in particular, that the determination of the equilibrium conditions between the melt and bcc modification of the iron crystal is a separate specific problem in atomistic simulation, which can be solved with the help of quantum molecular dynamics calculations [24]. Using the model of the phase field crystal, this problem is solved by analyzing free energy (1) in the one-mode approximation (2):

$$F = \int\left[(B_0^\ell - B_0^x)\frac{n^2}{2} - 2a\frac{n^3}{3} + 15v\frac{n^4}{4}\right]dV = \int B_0^x\frac{n}{2}(1+R_1^2\nabla^2)^2 n\,dV. \quad (31)$$

In this functional, we determine the values of coefficients B_0^ℓ, B_0^x, and R_1, as well as the values of parameters a and v for the bcc lattice of iron.

5.1. Parameters of the bcc Lattice of Iron

Let us now apply density functional theory [25–27], in which Eqs. (1) and (31) can be derived by expanding the Helmholtz free energy into a Taylor series in the vicinity of average atomic density $\overline{\rho}$ of the melt. Indeed, for the sum of potentials of the liquid and the crystal,

$$F = \int d\mathbf{r}[(l+n(\mathbf{r}))\ln(l+n(\mathbf{r})) - n(\mathbf{r})] - \frac{1}{2}\int d\mathbf{r}\int d\mathbf{r}' n(\mathbf{r})C^{(2)}(|\mathbf{r}-\mathbf{r}'|)n(\mathbf{r}') \quad (32)$$

we can use the expansion

$$(1+n)\ln(1+n) - n \approx \frac{1}{2}n^2 - \frac{2}{3}an^3 + \frac{15}{4}vn^4, \quad (33)$$

in which the coefficients are chosen so that they correspond to the coefficients in the free energy density in functional (31). Having determined these coefficients, we can calibrate the free energy functional for iron.

The free energy density in the second integral of expression (32) can now be written in the reciprocal space of the k vectors in terms of the two-point correlation function for the crystal:

$$\frac{C^{(2)}(k)}{\overline{\rho}} \approx -C_0 + C_2k^2 - C_4k^4. \quad (34)$$

Coefficients C_0, C_2, and C_4 are required to fit the functional to the first peak of the pair correlation function in the space of k vectors; the structural factor is defined as

$$S(k) = 1/[1 - \overline{\rho}C(k)], \quad (35)$$

where $C(k)$ is the correlation function. Then functional (32) with allowance for expressions (33) and (34) assumes the form

$$F \approx \int\left(\frac{n^2}{2} - 2a\frac{n^3}{3} + 15v\frac{n^4}{4}\right)dV + \int\left[\frac{n}{2}(\overline{\rho}C_0 + \overline{\rho}C_2\nabla^2 + \overline{\rho}C_4\nabla^4)n\right]dV, \quad (36)$$

which can easily be transformed to

$$F \approx \int\left(\frac{1+\overline{\rho}C_0}{2}n^2 - 2a\frac{n^3}{3} + 15v\frac{n^4}{4}\right)dV + \int\frac{\overline{\rho}C_2^2}{8C_4}n\left(4\frac{C_4}{C_2}\nabla^2 + 4\frac{C_4^2}{C_2^2}\right)n\,dV. \quad (37)$$

Let us introduce the coefficients

$$B_0^\ell = 1 + \overline{\rho}C_0, \quad B_0^x = \overline{\rho}C_2^2/4C_4, \quad R_1 = \sqrt{2|C_4|/C_2}, \quad (38)$$

where, as before, R_1 is the scale of transformation of the operators. Substituting this expression into (37), we finally obtain the functional

$$F \approx \int\left(B_0^\ell\frac{n^2}{2} - 2a\frac{n^3}{3} + 15v\frac{n^4}{4}\right)dV + \int B_0^x\frac{n}{2}(2R_1^2\nabla^2 + R_1^4\nabla^4)n\,dV, \quad (39)$$

which completely corresponds to free energy functional (1) or (31).

Using the results obtained in [15], we obtain the following values of the constants: $1/S(k_m) = 1 - C(k_m) = 0.332$ and $C''(k_m) = -10.40$ Å^2. Here, $S(k_m)$ is the structural factor (35) calculated for the critical wavenumber $k_m = 2.985$ Å^{-1}. Both k_m and coefficient $C''(k_m)$ determine the principal (first) peak of the correlation function and approximate the envelope of the atomic density of the unit cell in the bcc lattice of iron. In this case, we can define the coefficients of correlation function (34) as $C_0 = 10.9153/\overline{\rho}$, $C_2 = 2.6/\overline{\rho}$ Å^2, and $C_4 = 0.1459/\overline{\rho}$ Å^4 for reference density of iron melt $\overline{\rho} = 0.0801$ Å^{-3} [15, 18].

The parameters for functional (31) can now be written as

$$\Delta B_0 = B_0^\ell - B_0^x = 1 + \overline{\rho}(C_0 - C_2^2/4C_4), \quad (40)$$

$$a = \frac{3}{16S(k_m)u_s}, \quad v = \frac{4}{15\cdot 3\cdot 60S(k_m)u_s^2}, \quad (41)$$

where $S(k_m) = 3.012048$, $u_s = 0.72$ is the equilibrium value of the amplitude, and parameters B_0^x and R_1 are defined by expressions (38).

5.2. Conditions for the Existence of a Liquid and bcc Crystal

For convenience of further calculations, we introduce the following substitution in functional (31):

$$\tilde{n} = \sqrt{\frac{15v}{R_1^4 B_0^x}}\left(n - \frac{2a}{45v}\right),$$
$$\varepsilon = \frac{1}{R_1^4 B_0^x}\left(\frac{4a^2}{45v} - \Delta B_0\right), \tag{42}$$

where $\tilde{n}$ is the renormalized dimensionless density and ε is the relative temperature,

$$\varepsilon = \frac{T_c - T}{T}, \tag{43}$$

which determines the excess over transition temperature $T = T_c$ and the relation between elastic properties of the system in terms of quantities ΔB_0 and B_0^x. Then free energy (31) assumes a more convenient and compact form:

$$\Im = \int\left(\frac{\tilde{n}}{2}[-\varepsilon + (1+\nabla^2)^2]\tilde{n} + \frac{\tilde{n}^4}{4}\right)dV. \tag{44}$$

Passing from functional (31) to functional (44), we have assumed that all constants or linear contributions in $\tilde{n}$ can be omitted without loss of accuracy and correctness of analysis because these quantities make zero contribution to the equation of the phase field crystal model with the conservative order parameter, which in the stationary case has the form of Eq. (12). It should also be noted that coefficient R_1 is cancelled out in the derivation of free energy (44).

In the 3D case, the bcc structure can be represented in terms of equilibrium lattice parameter q_{eq} and lattice wavenumber $q = 2\pi/a_{\text{eq}}$, which are used for the reciprocal lattice vectors:

$$\mathbf{q}_1 = \frac{q}{2}(\mathbf{i}_1 + \mathbf{i}_2 - \mathbf{i}_3),$$
$$\mathbf{q}_2 = \frac{q}{2}(\mathbf{i}_1 - \mathbf{i}_2 + \mathbf{i}_3), \tag{45}$$
$$\mathbf{q}_3 = \frac{q}{2}(-\mathbf{i}_1 + \mathbf{i}_2 + \mathbf{i}_3),$$

where $\mathbf{i}_1$, $\mathbf{i}_2$, and $\mathbf{i}_3$ are unit vectors. Then general solution (13) with allowance for relations (45) has the amplitude representation of the bcc structure in the form

$$\tilde{n} = n_0 + 4\eta[\cos(qx)\cos(qy) + \cos(qx)\cos(qz) + \cos(qy)\cos(qz)]. \tag{46}$$

Free energy (44) with allowance for this relation for the unit cell of the bcc lattice assumes the form

$$F(\tilde{n},T) = \int_0^{2\pi/q}\frac{q}{2\pi}dx\int_0^{2\pi/q}\frac{q}{2\pi}dy\int_0^{2\pi/q}\frac{q}{2\pi}dz \times\left[(1-\varepsilon)\frac{\tilde{n}^2}{2} + \frac{\tilde{n}}{2}(2\nabla^2 + \nabla^4)\tilde{n} + \frac{\tilde{n}^4}{4}\right]. \tag{47}$$

Minimizing free energy (47) in wavenumber q, we obtain its equilibrium values $q_{\text{eq}} = 0$, $\sqrt{2}/2$, $-\sqrt{2}/2$. Substituting now the positive root of wavenumber $q = q_{\text{eq}} = \sqrt{2}/2$ into expression (47) for the free energy and integrating, we obtain

$$F_{\text{bcc}}(n_0,\eta) = \eta^2(18n_0^2 - 6\varepsilon) + 48\eta^3 n_0 + 135\eta^4 + \frac{n_0^2}{2}(1-\varepsilon) + \frac{n_0^4}{4}, \tag{48}$$

where subscript "bcc" indicates the structure of the bcc lattice. Minimizing further expression (48) in amplitude η, we get

$$\frac{\partial F_{bcc}(n_0,\eta)}{\partial\eta} = \eta(-12\varepsilon + 36n_0^2) + 144\eta^2 n_0 + 540\eta^3 = 0. \tag{49}$$

This equation has the following roots:

$$\eta = 0; \quad -\frac{2n_0}{15} \pm \frac{\sqrt{-11n_0^2 + 5\varepsilon}}{15}. \tag{50}$$

From the set of solutions (50), we choose the positive root and substitute it into Eq. (48). As a result, we obtain the final form of free energy functional $F_{\text{bcc}}(n_0, \Delta B_0)$ of the bcc lattice structure.

To construct the structural diagram in the liquid–bcc crystal system, we write the Maxwell area rule (analogously to Eqs. (30)):

$$\mu_{\text{bcc}}(n_{0\text{bcc}},\varepsilon) = \mu_h(n_{0h},\varepsilon),$$
$$F_{\text{bcc}} - F_h = \mu_h(n_{0h},\varepsilon)(n_{0\text{bcc}} - n_{0h}). \tag{51}$$

Here, free energy F_h and chemical potential $\mu_h = \partial F_h/\partial n|_{n=n_{0h}}$ of the liquid are defined by expression (17) taking into account its dimensionless form. Solving system (51) for the average density $n_{0\text{bcc}}$ of the bcc structure and average density n_{0h} of the homogeneous structure, we obtain the domains of existence of densities $\tilde{n}$ of liquid iron of bcc iron crystal for various temperatures ε.

Figure 5 shows the domains of existence of the homogeneous liquid phase and the crystalline bcc structure in "normalized average atomic density $\tilde{n}$ vs. dimensionless temperature ε" coordinates as the solution to system of equations (51). Obviously, while determining various vectors (45) in solution (13) (e.g., for a face-centered or hexagonal closely packed lattice), we must supplement the diagram in Fig. 5 with the domains of existence of these 3D structures. This is confirmed by numerically solving the 3D time-dependent equation of the phase field crystal [28].

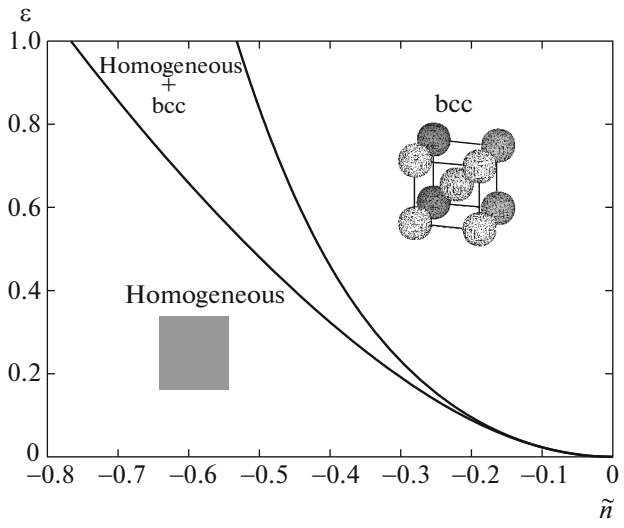

Fig. 5. Diagram of coexistence of a 3D homogeneous liquid and bcc lattice in coordinates of dimensionless temperature ε vs. dimensionless average density $\tilde{n}$.

Using the values of parameters (40) and (41), as well as transformations (42), we can reconstruct the diagram in Fig. 5 for dimensional quantities and parameters; in particular, the temperature of the equilibrium coexistence of the iron melt and its high-temperature crystalline bcc modification is determined.

6. FEATURES OF APPROXIMATION OF THE PHASE FIELD MODEL

6.1. Common Features of Models

The phase field crystal (PFC) model used here is based on an analysis of free energy (1) in the Brazovskii sense [5]. This form of free energy makes it possible to describe the transition to the periodic state and is formally (analytically) identical to the form required for constructing the weak crystallization theory (WCT). Both theories describe the first-order transition due to the presence of the cubic term in free energy density (4) as shown in Section 2. With such a formal generality, these two theories contain similar solutions. For example, for the 2D space, we observe that (i) isotropic phases (solutions for the liquid) are completely identical; (ii) the hexagonal crystalline phase in the WCT [29] corresponds to the triangular structure in the PFC model (see Section 3.2); finally (iii), the smectic phase in the WCT [29] as a phase with one-dimensional modulation of the atomic density corresponds to the striped structure in the PFC model (see Section 3.3).

For the short-wavelength field of the atomic density in the WCT, as well as for the long-wavelength field in the PFC model, coefficients a and v in expansion (4) can be assumed variable but dependent on the wavevectors of different directions in the crystal lattice [6, 30]. For example, coefficient v in the general case depends on the angles between the wavevectors of the directions in the lattice. In this case, the structural diagram can become richer and more diversified than those obtained in this study. In particular, it can be observed that [6] (i) the diagram of 2D structures shown in Fig. 4 is supplemented with possible types of a quasi-crystal lattice of the icosahedral type; (ii) minimization of the free energy in the angles between the wavevectors supplements the diagram of 3D structures (see Fig. 5) with various bcc lattice types, columnar and bent structures, as well as with lattices of the rhombohedral and face-centered modifications (as in the liquid–smectic phase transitions [31]).

6.2. Differences between the WCT and the PFC Model

However, the theoretical approximations in the WCT and in the PFC model are different. In particular, the solutions in the WCT are real-valued solutions for short-wavelength 3D processes in contrast to solutions in the PFC model describing the periodic structure with information on elasticity, dislocations, etc., on larger scales. In this sense, the PFC model is the long-wavelength theoretical description (like any other phase field model [13]), in which predictions on short-wavelength scales are not theoretically exact nor reliable for applications. Indeed, the WCT presumes that the solutions hold in the range of order parameter $n \approx \rho_{short}/\rho$, where ρ is the long-wavelength component of density and ρ_{short} is its short-wavelength component [32]. The solutions and structural diagrams in the WCT (see, e.g., [33]) are analyzed for $n_0 = 0$ (zero mean field in the liquid) and $n_0 \neq 0$ (nonzero mean field corresponding to periodic modulation of density with the lattice period in crystalline substances [32] or of the molecular spacing in smectics [34]). This definition implies smallness of the mean value appearing near the weak-crystallization phase transition: $n_0 \ll 1$. Conversely, the long-wavelength nature of determining the order parameter in the PFC model as the relative difference between the local atomic density and the density of the liquid, $n \equiv (\rho - \overline{\rho})/\overline{\rho}$, makes it possible to consider the solution for the mean value $n_0 > 0$ without confining analysis to values much smaller than unity.

The contribution of the cubic term in free energy (4) in the WCT is small in view of the smallness of parameter a. Density jump (11) at the phase transition point is small (because $\Delta n \propto a$), and the transition itself becomes nearly continuous. In this case, the contribution from thermodynamic fluctuations is of fundamental importance for the initiation and continuation of crystallization. In this sense, we are talking about crystallization as a "weak transition," in which thermodynamic fluctuations considerably affect its dynamics and the structural diagram [30]. Collaterally with this theory, the PFC model also takes into

account the fact that crystallization can be described for an appreciable value of parameter a, significant value of density jump (11), and a weak effect of thermodynamic fluctuations in the crystallization proper. Therefore, the PFC model also makes it possible to describe crystallization as a "strong transition."

6.3. Role of Fluctuations in the WCT and in the PFC Model

The solutions and structural diagrams for the PFC model considered above (see Sections 3 and 4) were obtained in the mean field approximation. This obviously implies disregard of fluctuations in the system.

In the PFC model, fluctuations should be involved in the nucleation of a new phase [35] as well as (at least) in the initiation of the transformation dynamics (because a supercooled metastable liquid cannot solidify without fluctuations in the strong crystallization theory also). For the further evolution of the process, fluctuations can be omitted when analyzing the solutions of the PFC model, because coefficient $2a$ of the cubic term in energy density (4) can be not small as compared to unity [14]. Indeed, coefficient $2a/3$ determines the height of the barrier between the phases and substantially increases the depth of the minima in the free energy density for $2a/3 \sim 1$, reduces the role of thermodynamic fluctuations, but increases the role of the driving force of the liquid–crystal transition.

Conversely to the PFC model, the WCT presumes that the additional condition for a nearly continuous first-order transition is precisely the smallness of the coefficient of the cubic term in free energy density (4) as compared to unity [6, 32]. In this sense, the role of thermodynamic fluctuations in the WCT becomes decisive upon a decrease in control parameter ΔB_0 (i.e., in the vicinity of the phase transition point).

Thermal fluctuations play a special role in the WCT, because these fluctuations are associated with the occurrence of point defects that can disturb the intrinsic order of the structure. For example, analysis of the WCT for the 2D geometry of films shows [29] that dislocations and thermal fluctuations associated with them do not violate the order in the smectic phase on a scale of

$$L \lesssim r_c \exp(B_0^x / R_1^2 \Delta_g). \tag{52}$$

(Here and below, all expressions are given in the notation of parameters of free energy function (4) taking into account operator (2) for the one-mode approximation.) The stability scale L of a smectic, which is defined by condition (52), considerably exceeds radius r_c of the dislocation core because one of the conditions for the applicability of the WCT must be observed:

$$\frac{R_1^2 \Delta_g}{B_0^x} \ll 1. \tag{53}$$

In this condition, gap Δ_g in the fluctuation region can be estimated as [6]

$$\Delta_g \sim \left(\frac{T^2 v^2}{B_0^x R_1^6} \right)^{1/3}, \tag{54}$$

or, with allowance for the relations between the parameters of the theory (see Section 2.3.4 in review [6]), we obtain

$$\Delta_g \sim a \left(\frac{T}{B_0^x R_1^3} \right)^{1/3}. \tag{55}$$

Conditions (52)–(55) show that with increasing temperature T, stability scale L of the smectic ordered phase decreases. On scales larger than L, the translational order of the smectic phase is violated and it can become, e.g., a homogeneous phase [29].

The smectic phase with the translational symmetry corresponds to the striped structure in the PFC model (see Section 3.3). Analyzing thermal fluctuations similarly to [6, 29] in the PFC model, we can estimate the effect of dislocations on disordering of the striped structure. Substituting expression (55) into the stable scale condition (52), we obtain

$$L \lesssim r_c \exp\left(\frac{(B_0^x)^{4/3}}{a R_1 T^{1/3}} \right)^{1/4}. \tag{56}$$

In the long-wavelength PFC model, parameter a can be not small (comparable with unity); in this case, stability scale (56) decreases with increasing parameter a in accordance with the exponential law $L \sim r_c \exp(a^{-1/4})$. This effective spatial deterioration of the stability of the striped structure to thermal fluctuations is a quite natural result, which obviously demonstrates the difference between the short-wavelength description in the WCT and the long-wavelength description of the PFC model.

6.4. Theory of 2D Melting and PFC Model

The diagram of 2D structures constructed in Fig. 4 from analysis of free energy (1) predicts stable structures formed during crystallization and melting in the PFC model. Fixing control parameter ΔB_0 in the diagram in Fig. 4, we can trace the variation in the structure upon an increase in average atomic density n_0 in the case of crystallization or its decrease during melting. In both cases, the transformation described by the change in free energy (1) is determined by the scenario of the first-order phase transition, in which atomic density n experiences discontinuity and changes jumpwise immediately at the phase transition point. Indeed, the discontinuous variation in density n described by expression (11) characterizes melting in 3D systems [36–38]. However, as applied to the 2D case, numerous experiments evidence continuity of melting of 2D films as a second-order phase transition

(see Part IV in review [39]). For this reason, 2D melting is described using the scenario of the Berezinsky–Kosterlitz–Thouless phase transition (BKT theory), which was initially formulated and developed for a continuous superfluid liquid–normal liquid transition in a helium-4 film [40–43]. The BKT theory is widely used in analyzing and interpreting experimental data (e.g., to interpret the dynamic properties of thin films [44] and estimate the superconducting state of single crystals [45]).

In the BKT theory, the melting process is described as a dual sequence of continuous variation in the topological order in the solid phase of the film [46]. During initial heating, dissociation of dislocation pairs takes place, which transforms the crystal into the hexatic phase having the liquid-crystal structure with the formation of disclinations. Subsequent dissociation of the formed disclination pairs upon a further increase in temperature leads to the formation of the isotropic liquid phase. This scenario is used in the BKT theory, e.g., to analyze melting over the boundaries of 2D grains by introducing two order parameters responsible for two different types of topological defects (dislocations and disclinations).

Melting over grain boundaries on dislocations was also described using numerical simulation of equations in the PFC model [2, 47, 48]. This made it possible to determine the equilibrium and metastable configurations of grain boundaries as soon as the crystal symmetry, elastic/plastic effects, and dislocations were taken into account in the PFC model. In particular, numerical simulation of the motion of dislocations has made it possible to determine the mechanism of grain-boundary melting in 3D samples [47]. Each isolated dislocation moves, melting the boundary in the radial direction from its core, because the localized excess of elastic energy is inversely proportional to the radius of melting in accordance with a power law. The motion of dislocations continues until adjacent "preliminarily melted" regions within grain boundaries merge together. Such a description was obtained with discontinuous variation in the order parameter at the phase transition point, which coincides with the description of the atomistic mechanism of melting induced by structural disordering over grain boundaries [38, 49]. Moreover, the mechanism revealed in the simulation generally confirms the phenomenological scheme of melting and the experimental results for 3D metal samples [50]. The melting mechanism in 2D systems and the possibility of continuous variation in the atomic density in accordance with the conclusions of the BKT theory can be the subject of subsequent analysis based on the PFC model. Thus, analysis of the BKT theory and the PFC model shows that melting in 2D and 3D systems is fundamentally different both as regards the mechanism itself and the conditions of continuity (discontinuity) of variation in the order parameter (see review [39] and literature therein).

Note lastly that the simultaneous description of the structure and microscopic defects based on amplitude equations (13) is one trend in the development of the PFC model. In particular, multiscale analysis for stress-induced fusion of heteroepitaxial monatomic layers was carried out in [8]. The formation of the structure was described on micrometer lengths, but taking into account the microscopic effects with nanoresolution on atomic scales and with allowance for mismatch of atomic lattices of the monolayer and the substrate. In this case, quantitative predictions of superstructures (stripes, honeycombs, and triangles) were obtained for two metal systems (Cu on Ru(0001) and Cu on Pd(111)) in conformity with experimental data (see Figs. 3 and 4 in [8]). Therefore, to take into account microscopic defects in a mesoscopic dynamic structure, the equations of the PFC model should be combined with their amplitude representations (see analytic and numerical solutions in [14] and literature therein).

7. CONCLUSIONS

We have proposed and developed a method using the atomic density functional to describe equilibrium structures. Using this method, the free energy functionals for homogeneous, triangular, and striped 2D (planar) structures have been derived. Using the Maxwell thermodynamic rule, we constructed the structural diagram in a wide range of the control parameters. The proposed method makes it possible to extend the diagrammatic description to the case of 3D structures (e.g., a body-centered crystal lattice (see Fig. 2) and rod structure (see Fig. 3)).

Using the method developed here, we constructed the diagram of 3D structures for the equilibrium coexistence of the homogeneous liquid phase and the body-centered iron lattice. The free energy functional has been derived from density functional theory. The phase field crystal model has been qualitatively compared with the weak crystallization theory and the conclusions of the 2D melting theory.

ACKNOWLEDGMENTS

We thank Kenneth Elder for constant helpful discussions on the topic of this study.

This work was supported financially by the Russian Foundation for Basic Research (project no. 14-29-10282-ofi_m). The research of one of the authors (N.V.K.) was financed by the Russian Foundation for Basic Research (project no. 13-02-01149A).

REFERENCES

1. K. R. Elder, M. Katakowski, M. Haataja, et al., Phys. Rev. Lett. **88**, 245701 (2002).
2. K. R. Elder and M. Grant, Phys. Rev. E **70**, 051605 (2004).

3. K. R. Elder, N. Provatas, J. Berry, et al., Phys. Rev. B **75**, 064107 (2007).
4. L. D. Landau, Phys. Z. Sov. **11**, 26 (1937).
5. C. A. Brazovskii, Sov. Phys. JETP **41**, 85 (1975).
6. E. I. Kats, V. V. Lebedev, and A. R. Muratov, Phys. Rep. **228**, 1 (1993).
7. H. Zhang and K. Jiang, Discrete Contin. Dyn. Syst. B **19**, 607 (2014).
8. K. R. Elder, G. Rossi, P. Kanerva, et al., Phys. Rev. Lett. **108**, 226102 (2012).
9. P. Galenko, D. Danilov, and V. Lebedev, Phys. Rev. E **79**, 051110 (2009).
10. P. K. Galenko and K. R. Elder, Phys. Rev. B **83**, 064113 (2011).
11. H. Emmerich, H. Lo[umlaut]wen, R. Wittkowski, et al., Adv. Phys. **61**, 665 (2012).
12. P. K. Galenko, H. Gomez, N. V. Kropotin, et al., Phys. Rev. E **88**, 013310 (2013).
13. N. Provatas and K. Elder, *Phase-Field Methods in Materials Science and Engineering* (Wiley-VCH, Weinheim, 2010).
14. P. K. Galenko, F. I. Sanches, and K. R. Elder, Phys. D: Nonlin. Phenom. **308**, 1 (2015).
15. K.-A. Wu and A. Karma, Phys. Rev. B **76**, 184107 (2007).
16. K. R. Elder, Zh.-F. Huang, and N. Provatas, Phys. Rev. E **81**, 011602 (2010).
17. Zh.-F. Huang, K. R. Elder, and N. Provatas, Phys. Rev. E **82**, 021605 (2010).
18. A. Jaatinen, C. V. Achim, K. R. Elder, et al., Phys. Rev. E **80**, 031602 (2009).
19. E. Asadi and M. A. Zaeem, Comput. Mat. Sci. **105**, 110 (2015).
20. K.-A. Wu, A. Adland, and A. Karma, Phys. Rev. B **81**, 061601 (2010).
21. E. Asadi, M. A. Zaeem, and M. I. Baskes, JOM **66**, 429 (2014).
22. Feng Duan and Jin Guojun, *Introduction to Condensed Matter Physics* (World Scientific, Singapore, 2005), Vol. 1.
23. J.-C. Tolédano and P. Tolédano, *The Landau Theory of Phase Transitions* (World Scientific, Singapore, 1987).
24. D. Alfe, M. J. Gillan, and G. D. Price, Nature **401**, 462 (1999).
25. T. V. Ramakrishnan and Y. Yussouff, Phys. Rev. B **19**, 2775 (1979).
26. R. Evans, Adv. Phys. **28**, 143 (1979).
27. Y. Singh, Phys. Rep. **207**, 351 (1991).
28. J. Bueno, I. Starodumov, H. Gomez, et al., Comput. Mat. Sci. (2015).
29. V. V. Lebedev and A. R. Muratov, Sov. Phys. Solid State **32**, 493 (1990).
30. S. A. Brazovskii, I. E. Dzyaloshinskii, and A. R. Muratov, Sov. Phys. JETP **66**, 625 (1987).
31. E. I. Kats, V. V. Lebedev, and A. R. Muratov, Sov. Phys. Solid State **30**, 775 (1988).
32. V. V. Lebedev, *Fluctuation Effects in Macrophysics* (MTsNMO, Moscow, 2004) [in Russian].
33. I. Ya. Erukhimovich, JETP Lett. **63**, 459 (1996).
34. E. I. Kats, V. V. Lebedev, and A. R. Muratov, Sov. Phys. Solid State **31**, 102 (1989).
35. G. I. Töth, G. Tegze, T. Pusztai, et al., J. Phys.: Condens. Matter **22**, 364101 (2010).
36. T. V. Ramakrishnan, Phys. Rev. Lett. **48**, 541 (1982).
37. H. Kleinert, Phys. Lett. A **95**, 381 (1983).
38. S. T. Chui, Phys. Rev. B **28**, 178 (1983).
39. K. J. Strandburg, Rev. Mod. Phys. **61**, 161 (1988).
40. V. L. Berezinskii, Sov. Phys. JETP **32**, 493 (1970).
41. V. L. Berezinskii, Sov. Phys. JETP **34**, 610 (1972).
42. J. M. Kosterlitz and D. J. Thouless, J. Phys. C: Solid State Phys. **5**, L124 (1972).
43. J. M. Kosterlitz and D. J. Thouless, J. Phys. C: Solid State Phys. **6**, 1181 (1973).
44. V. M. Svistunov, A. I. D'yachenko, V. Yu. Tarenkov, et al., JETP Lett. **33**, 259 (1981).
45. M. A. Vasyutin, A. I. Golovashkin, and N. D. Kuz'michev, Phys. Solid State **48**, 2250 (2006).
46. B. I. Halperin and D. R. Nelson, Phys. Rev. Lett. **41**, 121 (1978).
47. J. Berry, K. R. Elder, and M. Grant, Phys. Rev. B **77**, 224114 (2008).
48. J. Mellenthin, A. Karma, and M. Plapp, Phys. Rev. B **78**, 184110 (2008).
49. D. S. Fisher, B. I. Halperin, and R. Morf, Phys. Rev. B **20**, 4692 (1979).
50. M. E. Glicksman and C. L. Vold, Surf. Sci. **31**, 50 (1972).

Translated by N. Wadhwa